

# Suppression of Dwarf Galaxy Formation by Cosmic Shocks

Filippo Sigward,<sup>1</sup> Andrea Ferrara<sup>2</sup> & Evan Scannapieco<sup>3</sup>

<sup>1</sup>Università di Firenze, Dipartimento di Astronomia e Scienza dello Spazio, Largo Enrico Fermi 5, 50125 Firenze, Italy

<sup>2</sup>SISSA / International School for Advanced Studies, Via Beirut 4, 34014 Trieste, Italy

<sup>3</sup>Kavli Institute of Theoretical Physics, University of California, Santa Barbara, CA 93106, USA

20 March 2024

## ABSTRACT

We carry out a numerical study of the effects of supernova-driven shocks on galaxy formation at  $z = 9$ . These "cosmic explosions" can have a significant impact on galaxies forming nearby. We study such interactions in two key cases. In the first case in which the forming galaxy has already virialized, the impinging shock has only a small effect ( $< 1\%$  of the gas is removed) and star formation continues relatively unimpeded. However, in the second case in which the nearby forming galaxy is at the more disruptive turn-around stage, a large fraction ( $\sim 70\%$ ) of the gas is stripped away from the host dark-matter halo and ejected into the intergalactic medium. As the time spent near turn-around is much longer than the interval from virialization to galaxy formation due to strong radiative losses, we expect the second case to be more representative of the majority of outflow-galaxy interactions. Thus SN-driven pregalactic outflows may be an efficient mechanism for inhibiting the formation of neighbouring galaxies at high redshift. We briefly outline the possible cosmological consequences of this effect.

**Key words:** cosmology: theory | galaxies: formation | intergalactic medium | large-scale structure of universe

## 1 INTRODUCTION

In currently favoured cosmological scenarios, the formation of structure is a hierarchical process, in which small initial subunits merge and accrete diffuse material to form larger structures of ever increasing mass. For instance, in the popular Cold Dark Matter (hereafter CDM) cosmogony<sup>1</sup>, large numbers of objects with masses  $M = 10^8 h^{-1} M_\odot$  collapse at  $z = 9$  from  $2\sigma$  density fluctuations. In this collapse, the gas first falls inwards along with the dark matter, then shock-heats to the virial temperature ( $T_{\text{vir}} \sim 10^4$  K; see, however, Keres et al. 2004 who find that for low-mass objects a cold accretion mode can take place), condenses rapidly due to line cooling, and becomes self-gravitating. Subsequently, massive stars form, synthesize heavy elements, and explode as supernovae (SNe) after  $\sim 10^7$  yr, enriching the ambient medium. These processes may have been enhanced by primordial zero-metallicity stars (Population III stars) that may have been massive enough to ignite powerful pair-production SNe (e.g. Heger & Woosley (2002)), or generate large 'seed' black holes (Madau & Rees 2001).

Around a redshift of 10–15, early sub-galactic stellar systems, perhaps aided by a population of accreting black holes in their nuclei, generated the ultraviolet radiation and mechanical energy that reheated and reionized most of the hydrogen in the universe. The latest analysis of the data from the WMAP (Wilkinson Microwave Anisotropy Probe) satellite seems to suggest that this reionization took place at  $z_{\text{ion}} = 20^{+10}_{-9}$  (Kogut et al. 2003), requiring the production of ionizing photons to have been extremely efficient in high-redshift galaxies (e.g. Ciardi, Ferrara & White (2003)).

The history of this crucial stage in cosmic structure formation depends both on the power spectrum of small-scale density fluctuations and on a complex network of poorly understood "feedback" processes. A generic consequence of all hierarchical scenarios is a large deposition of energy by SNe in the shallow potential wells of early sub-galactic systems. This may have two main effects, depending on the efficiency with which halo baryons can cool and fragment into clouds and then into massive stars: (a) the disruption of the host (dwarf) galaxy { the most violent version of stellar feedback { (Larson 1974; Dekel & Silk 1986; Mac Low & Ferrara 1999); (b) the ejection of metal-enriched gas from the host galaxy and the subsequent early pollution of the intergalactic medium (IGM) (Tegmark, Silk & Evrard 1993; Cen & Ostriker 1999; Scannapieco & Broadhurst 2001; Madau, Ferrara & Rees 2001; Scannapieco, Fer-

<sup>1</sup> Throughout this paper we will assume a flat universe with total matter, vacuum, and baryonic densities in units of the critical density of  $\Omega_m = 0.3$ ,  $\Omega_\Lambda = 0.7$ , and  $\Omega_b = 0.05$  respectively, and a Hubble constant of  $H_0 = 100 h \text{ km s}^{-1} \text{ Mpc}^{-1}$ , with  $h = 0.65$ .

rara & Madau 2002; Springel & Hernquist 2003). Furthermore, the well-established presence of heavy elements such as carbon, nitrogen and silicon in the Ly forest clouds at  $z = 3-3.5$  provides strong evidence for such an early episode of pregalactic star formation and outflows (Songaila 2001; Pettini & Pagel 2004).

Similarly, stellar feedback and pregalactic outflows are likely to have efficiently inhibited high-redshift galaxy (and consequently star) formation. Because of the short cooling time of the gas in high- $z$  small halos, strong feedback has been advocated in hierarchical clustering scenarios to prevent a "cooling catastrophe" in which too many baryons are converted into stars at very high redshifts. The required reduction of the stellar birthrate in halos with low escape velocities may naturally result from the heating and expulsion of material by winds from massive stars and quasars, and multiple SN explosions.

It is also well known that the radiative and mechanical energy deposited by massive stars and accreting black holes into the interstellar medium of protogalaxies may have a more global negative feedback on galaxy formation. The photoionizing background responsible for the reionization of the IGM will have two effects: a gas pressure increase, preventing accretion into low-mass halos, and the reduction of the rate of radiative cooling of baryons inside the halos themselves (Efstathiou 1992; Thoul & Weinberg 1996; Navarro & Steinmetz 1997; Benson et al. 2001, 2002a,b, 2003). Furthermore, blast-waves produced by mini-quasars and protogalaxies propagate into the intergalactic space and may drive large portions of the IGM to a much higher adiabat than expected from photoionization (Voit 1996; Madau, Ferrara & Rees 2001; Theuns, Mo & Schaye 2001; Cen & Bryan 2001), so as to quench the collapse of further galactic systems by raising the cosmological Jeans mass.

In a complementary study, Benson & Madau (2003) have recently performed a detailed calculation of the effect of the increased gas pressure after this global early energy input into the IGM at the end of the cosmic dark ages. They have shown that preheating alone is not able to explain the sharp cut-off of the luminosity function at bright magnitudes and reproduce the observed abundance of satellite galaxies in the Local Group. It is worth noting that preheating consists of a homogeneous heat deposition in the IGM. Therefore, it affects galaxy formation in a global manner, through an increase in the filtering mass (Gnedin 2000).

In this paper we will be concerned with events of multiple supernovae in protogalaxies and the mechanical interaction of their shocks with neighbouring overdense regions. Considerable recent theoretical effort has gone into understanding the long-range feedback due to UV/ionizing radiation. Relatively less attention has been paid to the problem of how galaxy formation in these objects is hindered by shocks from nearby protogalaxies. However, limited analytic and numerical studies on a global cosmological scale have indicated that such interactions may have had an enormous impact on the galaxy luminosity function and its evolution (Scannapieco, Ferrara & Madau 2002; Hacker, Scannapieco & Davis 2002). While shock-cloud interactions within the interstellar medium have been simulated in detail (e.g. Klein, McKee & Coella (1994)), such related cosmological interactions have been largely neglected. Thus it is important to study this process in detail.

The structure of this paper is as follows: in §2 we outline the model used and the assumptions adopted in building up our model of "cosmic" stellar feedback; in §3 we describe the simulations carried out to examine the effects of SN explosions on a nearby halo, and in §4 we present our results and give a quantitative analysis. A summary is given in §5.

## 2 MODEL ASSUMPTIONS

We want to study the effect of cosmic explosions produced by SNe in a given (source) halo impinging onto a neighbouring (target) object on its way to collapse into a luminous galaxy. To address this problem in a numerical context, we make use of the hydrodynamic code CLAWPACK<sup>2</sup>, an explicit Eulerian, shock-capturing and upwind second-order Godunov (with TVD stability) method.

Our investigation is centered on the impact on an impinging shock during two main stages of collapse of the target halo: turnaround and virialization, both of which are described in further detail below. In both cases, we set the redshift of interaction to be  $z = 9$ , as a typical value during reionization, and the halo mass to  $M = 10^8 h^{-1} M_\odot$ , which is chosen both because of the ubiquity of such objects at  $z = 9$  (e.g. Scannapieco, Ferrara, & Madau 2002) and because they are able to quickly cool by atomic lines, regardless of the evolution of primordial  $H_2$  (Haiman, Rees, & Loeb 1997; Ciardi et al. 2000).

### 2.1 Gas distribution in the target halo

In constructing a model for the structural properties of the target halo, we neglect self-gravity of the baryons, which is motivated by the fact that  $\rho_b = \rho_m \approx 1$ . Therefore we consider the gas in hydrostatic equilibrium inside the gravitational potential of the dark matter halo.

#### 2.1.1 The virialized case

To determine how the baryons are arranged in the dark matter gravitational field, we must first determine the dark matter distribution inside pre-galactic systems. Here we assume that dark matter halos at virialization equilibrium follow the universal (spherically averaged) density profile determined by Navarro, Frenk & White (1997; hereafter NFW):

$$\rho(r) = \frac{\rho_m (1+z)^3}{c x (1+cx)^2}; \quad (1)$$

where

$$x = \frac{r}{R_{\text{vir}}};$$

$\rho_c$  is the critical density of the universe,  $R_{\text{vir}}$  the (physical) virial radius of the system (at which the mean enclosed density is 200 times the mean cosmic value  $\bar{\rho}_m = \rho_m (1+z)^3$ ),  $c$  is the halo concentration parameter,  $c = (200/3)c^3 = F$  (the characteristic overdensity, and

$$F(c) = \ln(1+c) - \frac{c}{1+c}; \quad (2)$$

<sup>2</sup> Conservation LAWS PACKAGE. Details can be found at <http://www.amath.washington.edu/~claw/>

The total mass of the halo within the virial radius and the mass within a radius  $r < R_{\text{vir}}$  are, respectively:

$$M = \frac{4}{3} 200 c_m (1+z)^3 R_{\text{vir}}^3; \quad (3)$$

and

$$M(r) = \int_0^r (r')^4 r'^{02} dr' = M \frac{F(cx)}{F(c)}; \quad (4)$$

Equation (1) allows us to calculate a circular velocity squared

$$v_c^2(r) = \frac{GM(r)}{r} = V_c^2 \frac{F(cx)}{xF(c)}; \quad (5)$$

where  $V_c = (GM/R_{\text{vir}})^{1/2}$  is the value at the virial radius. The work done by the gravitational force on the escaping gas is equal to the variation of its kinetic energy, therefore the gas at the radius  $r$  is able to escape provided it has a velocity (squared) larger than:

$$v_e^2(r) = 2 \int_r^{R_{\text{vir}}} \frac{GM(r')}{r'^2} dr' = 2V_c^2 \frac{F(cx) + cx(1+cx)}{xF(c)}; \quad (6)$$

in which the NFW profile is extrapolated to infinity. The escape speed is maximum at the center of the halo,  $v_e(0) = 2V_c^2 c = F(c)$ .

To proceed, we follow the algorithm described in the appendix of NFW, and compute the concentration parameter (or, equally, the characteristic density contrast  $c$ ) of dark matter halos as a function of their mass for our adopted cosmological model. The algorithm assigns to each halo of mass  $M$  identified at redshift  $z$  a collapse redshift  $z_{\text{coll}}$ , defined as the redshift at which half of the mass of the halo was first contained in progenitors more massive than some fraction of the total mass (Lacey & Cole 1994). The assumption that the characteristic density of a pre-galactic system is proportional to the critical density at the corresponding  $z_{\text{coll}}$  implies:

$$c(M; z) / \frac{1+z_{\text{coll}}}{1+z}^3; \quad (7)$$

Lower mass halos generally collapse at higher redshift, when the mean density of the universe is greater: for this reason, from the previous relation we deduce that low-mass systems, at any given time, are more centrally concentrated than massive ones. As an example, we report in the following table the values of  $z_{\text{coll}}$  and  $c$ , obtained for different halos identified at  $z = 9$ .

$M [M_{\text{h}}]$	$z_{\text{coll}}$	$c$
$10^7$	12.5	4.9
$10^8$	12.2	4.8
$10^9$	11.9	4.7

To study the impact of high-redshift cosmic explosions on objects at  $1+z \leq 10$  in detail, we will assume a "typical" concentration parameter of  $c = 4.8$ . At these epochs, the dark matter halo of a subgalactic system is characterized by a virial radius:

$$R_{\text{vir}} = 0.76 M_{\text{h}}^{1/3} h^{-1} \frac{1+z}{10} \text{ kpc}; \quad (8)$$

a circular velocity at virial radius:

$$V_c = 24 M_{\text{h}}^{1/3} h^{-1} \frac{1+z}{10} \text{ km s}^{-1}; \quad (9)$$

and a virial temperature:

$$T_{\text{vir}} = \frac{GM}{R_{\text{vir}}} \frac{m_p}{2k} = 10^{4.5} M_{\text{h}}^{2/3} h^{-1} \frac{1+z}{10} \text{ K}; \quad (10)$$

where

$$M_{\text{h}} = \frac{M}{10^8 M_{\text{h}}^{-1}};$$

and  $\mu$  is the mean molecular weight ( $\mu = 0.59$  for a fully ionized hydrogen/helium gas of primordial composition). The escape speed at the center is:

$$v_e(0) = 77 M_{\text{h}}^{1/3} h^{-1} \frac{1+z}{10} \text{ km s}^{-1}; \quad (11)$$

Note, however, that high-resolution N-body simulations by Bullock et al. (2001) seem to indicate that high-redshift halos are actually less concentrated than expected from the NFW prediction. If this is the case, we might slightly overestimate the values of the escape speeds from pre-galactic systems.

Having fixed the dark matter density distribution, we can establish the density profile of the baryons. If the gas collapses and virializes along with dark matter, it will be shock-heated to the virial temperature and will settle down to an isothermal profile (Makino, Sasaki & Suto 1998):

$$\rho_b(r) = \rho_0 e^{-A v_e^2(0) - v_e^2(r)}; \quad (12)$$

with

$$A = \frac{m_p}{2kT_{\text{vir}}};$$

Throughout this paper we make the assumption that the gas is distributed isothermally in virialized structures. The central density of the gas  $\rho_0$  is determined by the condition that the total baryonic mass fraction within the virial radius is equal to  $\rho_b = \rho_m$  initially:

$$\frac{\rho_0}{c(1+z)^3} = \frac{B(200=3) c^3 \rho_b e^B}{\int_0^c t^2 (1+t)^B dt} = 44000 \rho_b; \quad (13)$$

where  $B = 2c = F(c)$ . At the virial radius  $\rho_b(R_{\text{vir}}) = 0.00144 \rho_0$ .

### 2.1.2 The turn-around case

Once a positive density perturbation has collapsed, it continues to attract matter. Bound shells cease expanding with the Hubble flow, continue to turn-around, and consequently the mass of the perturbation grows by accretion of new material. This smooth accretion is generally called secondary infall in the literature, because particles fall onto an already formed object. In this case we make use of the results obtained by Bertschinger (1985). Since gravity has no preferred scale, we can find self-similar solutions for secondary infall and accretion onto an overdense perturbation. The behaviour of this infall depends on the nature of the gas (collisional or collisionless) and on central boundary conditions, such as the presence of a black hole in the core. In our situation, the collisional (baryonic) matter moves in the potential well generated by the dissipationless (dark-matter) component. The

radius of the shell that is turning around increases with time as  $t^{8/9}$ , while the mass within this radius increases as  $t^{2/3}$ . At large radii, both dark matter and baryonic components have the same density distribution, given by:

$$\rho(r) / r^{-9/4} : \quad (14)$$

At smaller radii, the main difference between the two components is the existence of a spherical shock that forms in the baryonic gas due to the collision of the infalling gas with the self-generated core. Since this gas is dissipative, infalling fluid elements are decelerated by passage through this shock and by post-shock pressure gradients, and come to rest at the center.

In this model, fluid motion is unchanged when parameters are conveniently scaled as  $r' = r/R_{ta}$ :

$$v(r;t) = \frac{R_{ta}}{t} \hat{v}(\hat{r}) \quad (15)$$

$$\rho_b(r;t) = \rho_{igm} \hat{\rho}(\hat{r}) \quad (16)$$

$$p(r;t) = \rho_{igm} \frac{R_{ta}^2}{t} \hat{p}(\hat{r}) \quad (17)$$

$$M_b(r;t) = \frac{4}{3} \rho_{igm} R_{ta}^3 \hat{M}(\hat{r}) \quad (18)$$

where  $v$ ,  $\rho_b$ ,  $p$ ,  $M_b$  are respectively the gas velocity, density, pressure and the mass at the distance  $r$  from the centre of the perturbation at the cosmological time  $t$ , while the same symbols with the "hat" represent the relative dimensionless quantities;  $R_{ta}$  is the turn-around radius and  $\rho_{igm}$  is the mean baryonic density of the intergalactic medium at the redshift of interest (see equation (20)). The shock is located at a fixed fraction of the turn-around radius,  $r_s = 0.347$  for a gas with  $\gamma = 5/3$ , and propagates outwards according to the scaling  $r_s / t^{8/9}$ . The total mass of the over-dense region within the turn-around radius is calculated with  $\hat{M}(\hat{r} = 1) = 5.6$  and with  $\rho_m$  instead of  $\rho_b$  in (18):

$$R_{ta} = \frac{3M}{4 \cdot 5.6 \rho_{c,m}}^{1/3} (1+z)^{-1} : \quad (19)$$

## 2.2 The intergalactic medium

The intergalactic medium around the simulated halo is considered to be homogeneous with a density  $\rho_{igm}$ :

$$\rho_{igm} = \rho_{c,b} (1+z)^3 = 1.88 \cdot 10^{-29} h^2 \rho_b (1+z)^3 \text{ g cm}^{-3} \quad (20)$$

corresponding to a numerical density of about  $4 \cdot 10^4 \text{ cm}^{-3}$  at redshift  $z = 9$ . Furthermore, we assign to the IGM a temperature of  $T = 10^4 \text{ K}$ , typical of a fully ionized medium. This value is explained by the observations of absorbing lines of the IGM in spectra of distant quasars (Rauch 1998). It follows that the sound speed is  $C_{igm} \approx 15 \text{ km s}^{-1}$ .

## 2.3 The shock wave

To determine the properties of the impinging shock, we adopt a thin-shell approximation. In this model, we require an estimate of the shock Mach number  $M$  and the thickness of the cooled shell. If radiative losses are small within the hot-bubble driving the cosmic explosion, the shock velocity can be approximated by a Sedov-Taylor blast-wave solution:

$$v_s = \frac{2K_k E^{1/2}}{3 \rho_{igm}} d^{-3/2} ; \quad (21)$$

where  $E$  is the total energy of the shock,  $K_k = 0.2$  (e.g. Scannapieco, Ferrara & Madau 2002) is the total-to-kinetic energy conversion efficiency, and  $K = 1.53$  is a constant obtained from the exact solution for  $\gamma = 5/3$ . As for the energy  $E$ , we assume that one supernova occurs for every  $100 M_\odot$  of baryons that went into stars (see, e.g., Gibson 1997), so the number  $N$  of supernovae driving the bubble is:

$$N = 5 \cdot 10^4 M_{8, sf} (\rho_m h)^{-1} ;$$

where  $sf$  is the initial star formation efficiency. The total energy of the shock is then:

$$E = 2 \cdot 10^{51} K N \text{ erg} ; \quad (22)$$

where  $2 \cdot 10^{51} \text{ erg}$  is the energy of each supernova, taking into account also the contribution from stellar winds. Assuming an initial star formation efficiency  $sf = 0.1$ , a value that is broadly supported by observations of high- $z$  IGM metals and the high- $z$  cosmic star formation rates (Ciardi et al. 2000; Barkana 2002; Scannapieco, Ferrara & Madau 2002), we can estimate  $N \approx 5000 \text{ M}^{-1}$  and thus  $E \approx 10^{55} K \text{ M}^{-1} \text{ erg}$  for typical dwarf galaxy-sized objects of mass  $M \approx 10^8 M_\odot$ .

We estimate the distance  $d$  in equation (21), i.e. the radius of the shock wave, as the mean spacing between halos of a mass scale  $M$ :

$$d = \frac{3M}{4 \rho_{c,m}}^{1/3} (1+z)^{-1} = 94 M_8^{1/3} (1+z)^{-1} \text{ kpc} ; \quad (23)$$

From equations (20), (22) and (23) we note that the value of  $v_s$  in equation (21) is independent of redshift and halo mass.

An alternative estimate relies on the fact that the mean number of halos within a distance  $r$  from another halo is:

$$\langle N_r \rangle = 4 \pi n \int_0^r r'^2 [1 + \xi(r')] dr' ; \quad (24)$$

where  $n$  is the average number density of halos and  $\xi$  is their two-point correlation function. Both these quantities can be estimated from the classic analytical peaks formalism (Press & Schechter 1976, hereafter PS; Bond et al. 1991; Mo & White 1996). Note that the average number density in this equation is far less than  $(\frac{4}{3} d^3)^{-1}$  as defined by equation (23). This is due to the fact that the mean separation between halos is much larger than the average distance between a halo and its closest neighbor, because they are clustered together into groups of objects that only occupy a fraction of the cosmological volume. From equation (24), we can compute the probability for a nearest neighbour to be at a distance  $r$  as  $P(r) = 1 - \exp[-(6\pi n r)]$  and the mean distance to the nearest neighbour as:

$$d = \int_0^\infty r \frac{dP}{dr}(r) dr : \quad (25)$$

In this case, approximating the physical density  $n$  as  $(1+z)^{-3}$  times the PS number density of  $\frac{dn}{d \ln M}$  ( $M = 10^8 M_\odot = h; z = 9$ ), and making use of the matter power spectrum from Eisenstein & Hu (1998), with  $\sigma_8 = 0.87$ , we obtain a distance of 14 kpc. The similarity of this (power-spectrum and redshift dependent) estimate with our more

straightforward approach, give us confidence that the distance 9.4 kpc as given by equation (23) is a reasonable estimate for interactions in which we are interested.

We have to assess now the value of the second parameter of interest for the shock wave, the thickness of the shell. Almost the totality of the gas swept up by the front is concentrated in a relatively thin layer and the density inside the layer is constant and equal to the density behind the front surface. We have also to consider the fraction of baryons removed from the outflowing galaxy: according to Mori, Ferrara & Madau (2002), we can take about the 60% of a system with the same mass scale  $M$  of interest. In conclusion we obtain for the thickness  $d$  of the shell, from conservation of mass:

$$d = d_s \frac{\rho_{\text{igm}}}{3} + \frac{0.6M_b}{4\rho_s d^2}; \quad (26)$$

where  $\rho_s$  represents the post-shock density (i.e. the density inside the layer), achieved with the usual well-known "jump conditions" ( $\rho_s \propto \rho_{\text{igm}}'$  for supersonic shocks).

### 3 SIMULATION RESULTS

In both virialized and pre-virialized cases, we consider a computational grid made of  $150 \times 150$  cells and set the boundary conditions as zero-order extrapolation, i.e. requiring that the flow of the matter runs only outward across all four borders. As mentioned above, in both cases we select a target halo mass of  $M = 10^8 h^{-1} M_\odot$  and redshift of  $z = 9$  as our fiducial model. Convergence tests with double spatial resolution of the grid ( $300 \times 300$  cells) have been made to ensure that the simulations provide reliable results: in all cases the answers are consistent.

#### 3.1 Virialized case

Let us first consider the virialized case. For our fiducial parameters the virial radius of the pre-galactic system, which is assumed to be spherically symmetric, is equal to 1.75 physical kpc and its virial temperature is  $T_{\text{vir}} = 12,490$  K. In this case, the spatial resolution of the computational grid is 43.3 pc. To determine the velocity at which the shock reaches the halo, we replace the distance  $d$ , in eq. (23) with:

$$d \rightarrow d^0 = d - R_{\text{vir}}; \quad (27)$$

as we are interested in the initial point of the collision, when the front first reaches the overdense region.

The simulation starts with the coordinates of the centre of the target halo placed at the point<sup>3</sup>  $(x_0; y_0) = (63; 75)$ , i.e. (2.7; 3.2) kpc, with a radius of 40 cells. Both the pre-galactic system and the intergalactic medium are at rest, and the shock wave is modeled as a plane wave, at  $x = 20$  cells, moving from the left towards the right, with an initial velocity of about  $214 \text{ km s}^{-1}$ . In this case, the numerical density  $n_s$  and the pressure  $p_s$  behind the shock are  $n_s = 4n_{\text{igm}} = 1.6 \times 10^{-3} \text{ cm}^{-3}$  and  $p_s \propto \rho_{\text{igm}} v_s^2$ ; respectively,

and the temperature of the post-shock gas reaches a value of  $6.2 \times 10^5$  K.

Let  $t = 0$  be the time referred to by the initial conditions. The final time of the simulation is then  $t = 58.2 \text{ M yr}$ , equal to about 3.6 times the shock crossing time of the halo, defined as:

$$t_{\text{cross}} = \frac{2R_{\text{vir}}}{v_s}; \quad (28)$$

Note that virialization is quite late in the evolution of the perturbation, and during our simulation time it is possible that star formation (and SNe) could occur inside this object. While, in this case, the dynamics of the system would become more complicated, we choose to ignore these effects and study the virialized case as an idealization of the last possible time at which baryonic stripping could prevent star formation in the collapsing object. Indeed, due to the short time between virialization and star formation, it is much more likely that baryonic stripping will occur prior to virialization, as we discuss in more detail below.

In Figure 1 we show the density and temperature fields at three key stages. Initially the shock wave travels towards the centre, compressing the gas. When the shock first reaches the system, it encounters a density slightly greater than 30 times that of the IGM. At this point, the velocity of the internal wave changes in direction and drops by a factor of approximately the square root of ratio of the halo  $\rho_b$  and IGM  $\rho_{\text{igm}}$  densities (Bychkov & Pikelner 1975):

$$v_{s,h} = \frac{v_{s,\text{igm}}}{(\rho_b/\rho_{\text{igm}})^{1/2}}; \quad (29)$$

where  $v_{s,h}$  and  $v_{s,\text{igm}}$  are the front velocities inside the halo and in the IGM respectively, which gives  $38 \text{ km s}^{-1}$ .

During the second stage, the shock velocity gradually decreases, according to equation (12) as it runs into denser regions. In particular, the front reaches  $M \approx 1$  close to the halo core and lapses into a sonic wave, mingling with the surrounding matter. At this time, the shock begins to sag and to form two symmetric extensions in which the baryons are accumulated.

In the meantime the outflow continues to propagate outside the halo, with a velocity greater than the velocity inside the cloud. The intergalactic gas has now a post-shock pressure of  $1.4 \times 10^{13} \text{ erg cm}^{-3}$ , more than 240 times the IGM pressure and about 6 times the baryonic pressure of the collapsed system at the virial radius.

Finally, at a time  $t = 50 \text{ M yr}$  the two "flux sides" join together again behind the halo, "embracing" the entire system. After this time it is unlikely that the mass inside the virial radius will be ejected by momentum transfer. The dynamics of the interaction then becomes quite complicated, due to the presence of reflections of shock waves which scatter in the perturbation.

In Figure 2 we show density and temperature profiles along the horizontal direction crossing the halo centre ( $y = 75$ ), at each of these three different stages (from top to bottom). These plots uncover the same trends Figure 1, and indicate that after the interaction the gas structure of the halo is only weakly modified, especially in the core, where it is nearly unchanged.

<sup>3</sup> Hereafter we will indicate the coordinate of the cell along the horizontal axis as  $x$  and the coordinate along the vertical axis as  $y$ .

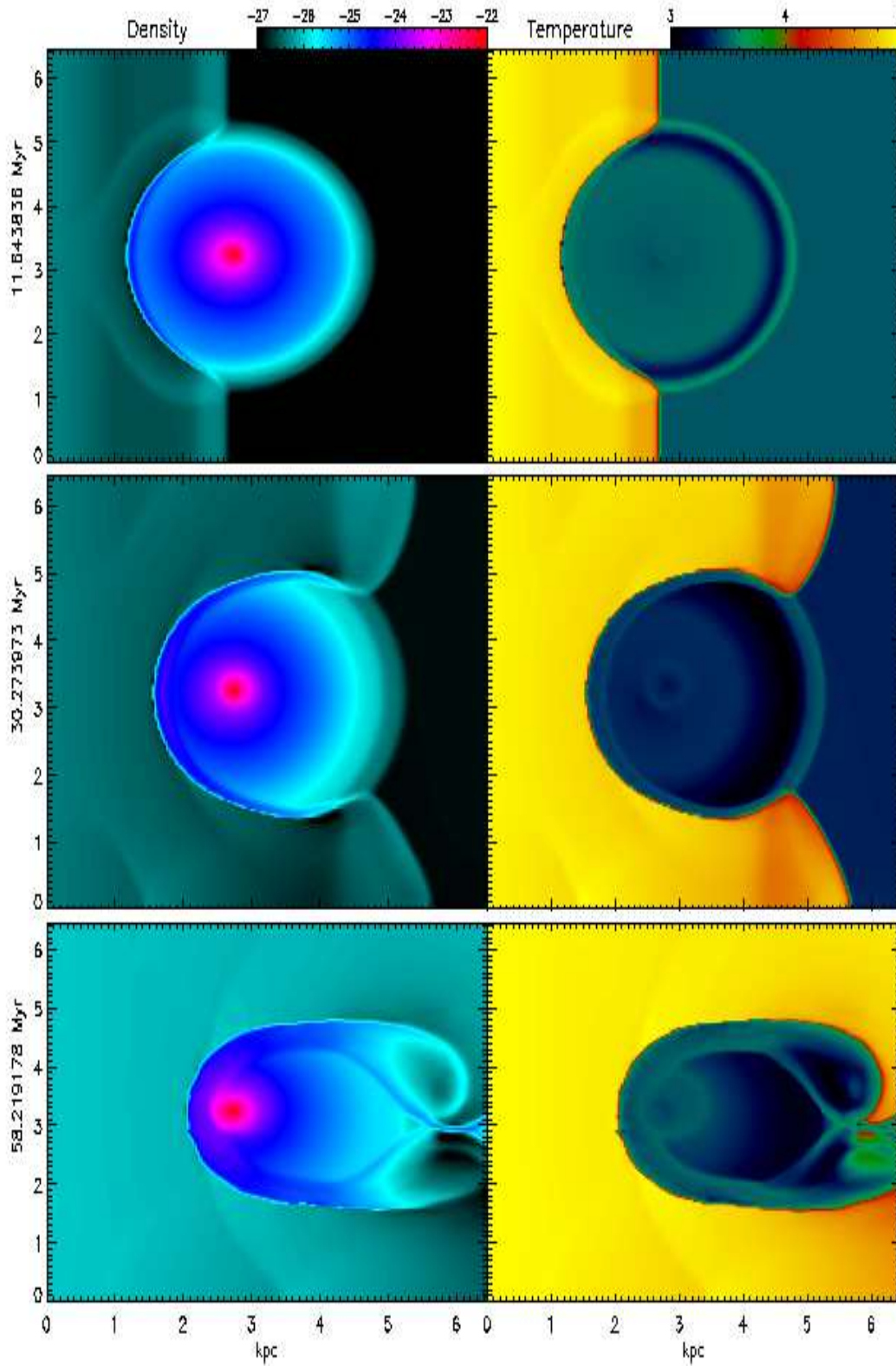


Figure 1. Snapshots of the dynamical evolution for the virialized halo case (NFW profile). Maps with logarithmic color scale are plotted for the density [ $\text{g cm}^{-3}$ ] (left) and temperature [K] (right) fields at three different times ( $t = 11.6$ ;  $30.3$ ;  $58.2$  Myr).

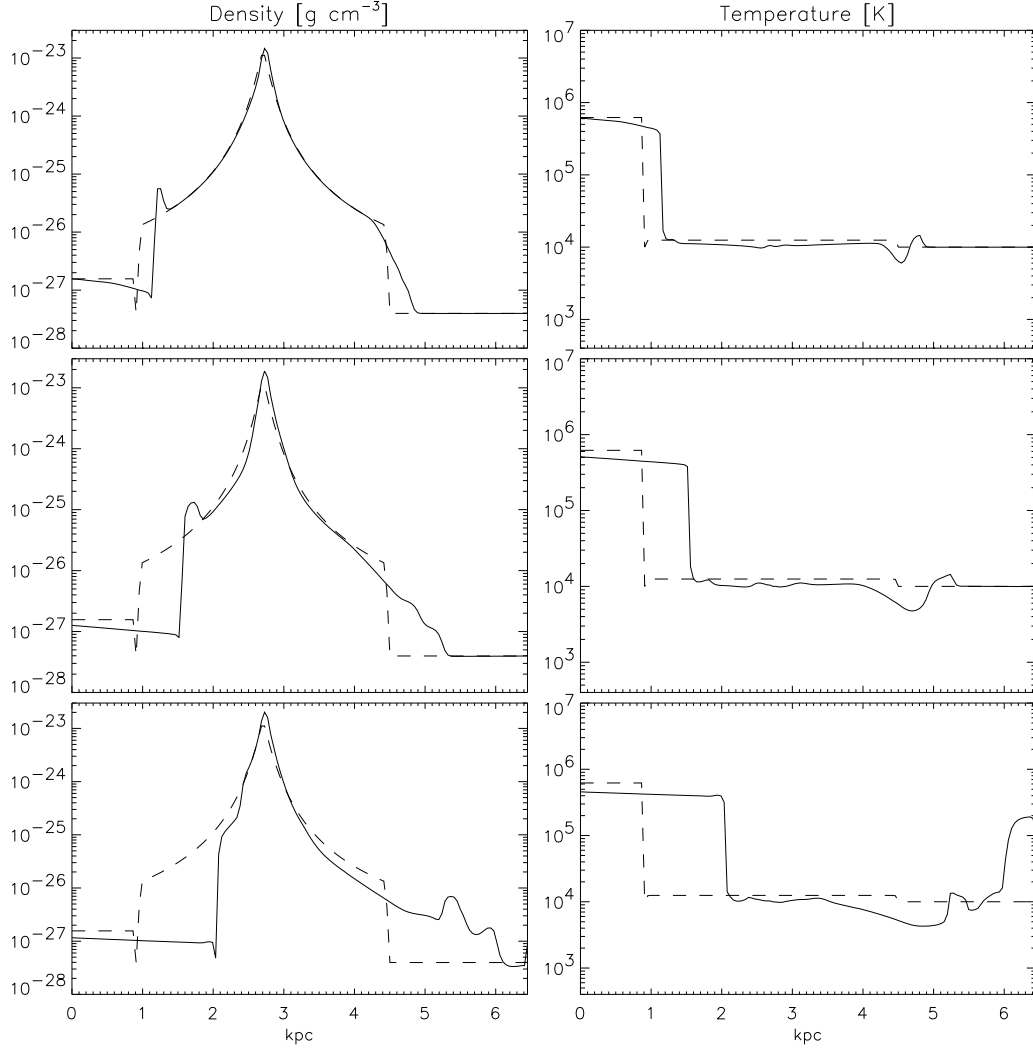


Figure 2. Virialized case. Density (left) and temperature (right) profiles for a horizontal cut crossing the centre of the halo ( $y = 75$ ), at times (from top to bottom)  $t = 11.6; 30.3; 58.2$  M yr. Dashed lines show the profiles for the same cut at the initial time.

### 3.2 Pre-virialized case

Let us move now to the pre-virialized case, when the halo is at the turn-around stage. Here the radius of our fiducial system, with the same mass and at the same redshift, is given by equation (19), which yields  $R_{ta} = 5.7$  kpc. Therefore, the Mach number of the shock wave given by equation (21) is larger than the previous value, and we obtain  $M = 37$  (i.e. a front expanding in the IGM with an initial velocity of roughly  $565 \text{ km s}^{-1}$  and with a crossing time of the halo  $t_{cross} \approx 19.8$  M yr) and  $d \approx 1.2$  kpc. The post-shock temperature of the gas reaches the value of  $T \approx 4.3 \times 10^6 \text{ K}$ . The new configuration of this problem consists of a spatial resolution of about 138 pc in the same  $150 \times 150$  computational grid. The centre of the overdense region is put at (49; 75) and its radius encloses 41 cells. The final time of the simulation is 133 M yr.

The dynamics (Figure 3) of this interaction, by and large, follow the same sequence discussed in the virialized case. Nevertheless some important differences can be seen. Note that at this stage the halo is not yet isothermal and

the solutions by Bertschinger (1985) expect values of pressure at the edge almost equal to those of the IGM, and a smoother decrease of the density with radius.

It follows that at this epoch the shock will be able to more easily penetrate into the centre of the perturbation. Figure 3 points out this fragility, showing that now the front is able to reach the halo core. For further details see also Figure 4, representing the evolution in time (from top to bottom) of the density and temperature profiles along the horizontal cut crossing the halo centre ( $y = 75$ ). The comparison between Figure 1 and Figure 3 emphasizes a morphological difference of the system.

## 4 QUANTITATIVE ANALYSIS

As the primary aim of our investigation is to assess the impact of galactic outflows on neighbouring overdense regions, it is important to quantify the amount of matter that can be removed from the halo. We follow the two criteria proposed by Scannapieco, Ferrara & Broadhurst (2000) to estimate

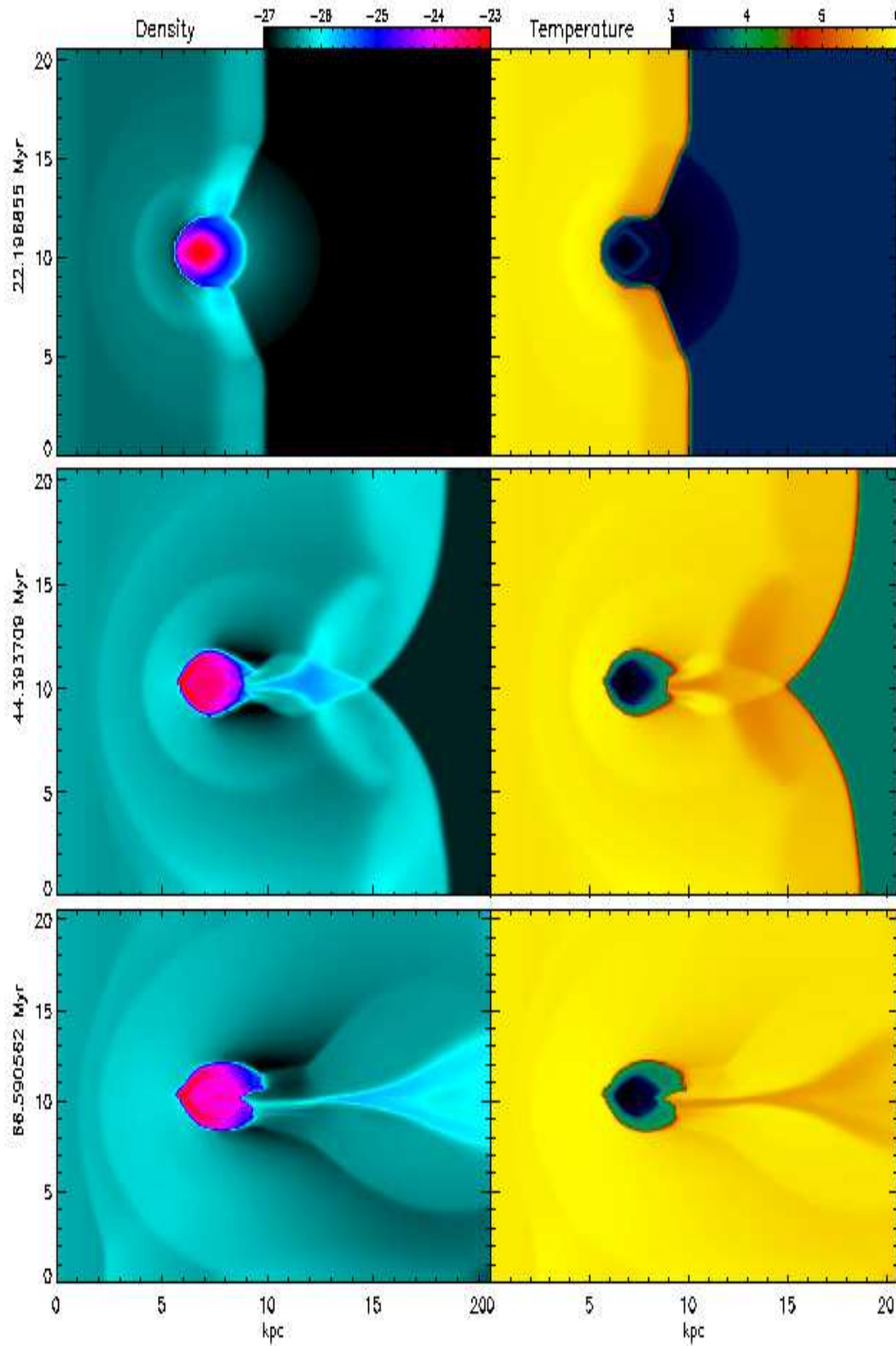


Figure 3. Snapshots of the dynamical evolution for the halo at the turn-around stage. Maps with logarithmic color scale are plotted for the density [ $\text{g cm}^{-3}$ ] (left) and temperature [K] (right) fields at three different times ( $t = 22.2$ ;  $44.4$ ;  $66.6$  Myr).



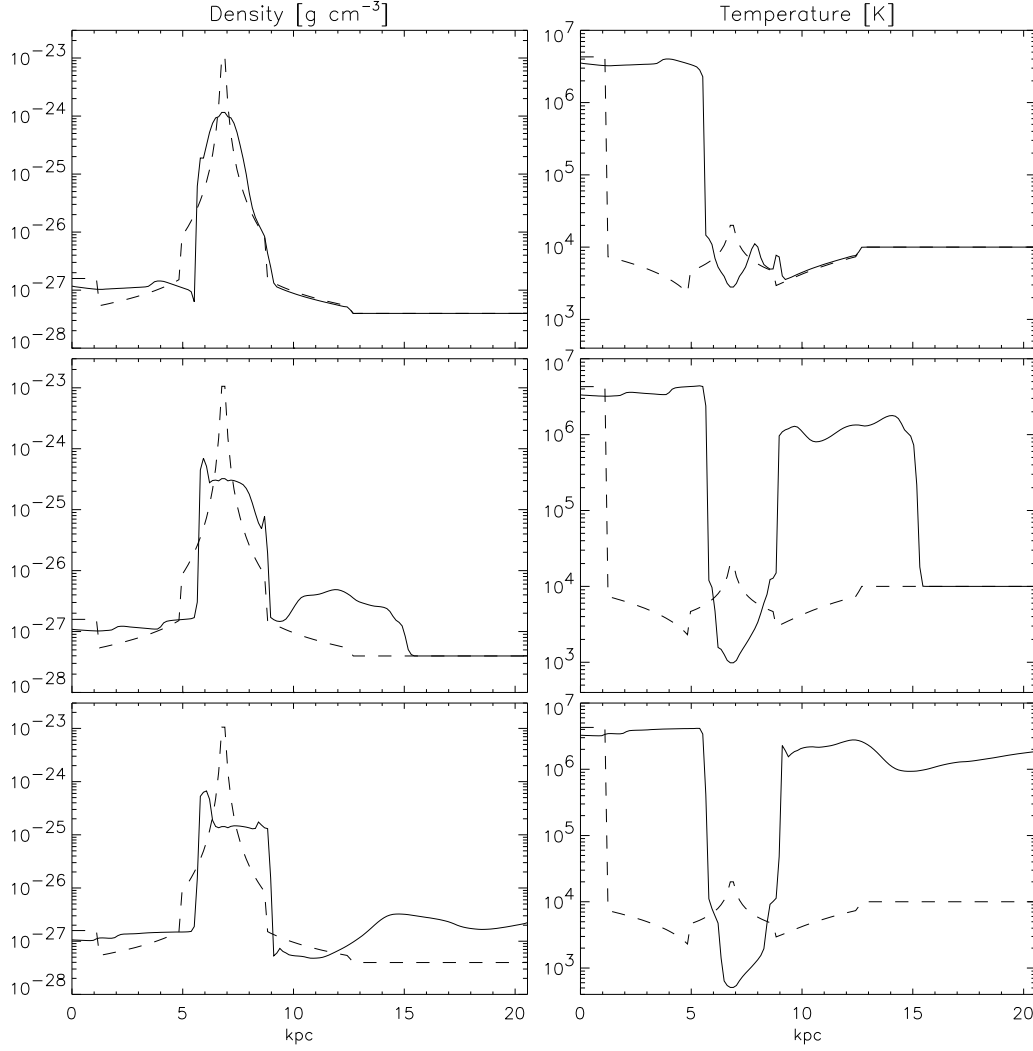


Figure 4. Turn-around stage. Density (left) and temperature (right) profiles for a horizontal cut crossing the centre of the halo ( $y = 75$ ), at times (from top to bottom)  $t = 22.2; 44.4; 66.6$  M yr. Dashed lines show the profiles for the same cut at the initial time.

this quantity. There are two mechanisms by which outflows from nearby objects can hinder the formation of a galaxy: in one case the gas is heated to a temperature greater than the virial temperature ("mechanical evaporation"), in the other case the shock transfers sufficient momentum to carry gas parcels out of the gravitational potential ("baryonic stripping").

Figure 5 shows, for the virialized case, the total fraction of baryonic mass removed from the virial radius of the halo (filled circles), by each of these mechanisms. The triangles (diamonds) represent the evolution of the fraction of mass with  $T > T_{\text{vir}}$  ( $v(r) > v_e(r)$ ), integrated over the halo. The first condition describes the importance of the mechanical evaporation, whereas the second one refers to baryonic stripping.

The physical interpretation of the behavior of the curves is as follows. The initial growth of the lines is due to the penetration of the shock into the outer layers of the halo, which are much less dense than the central core. Even at these large radii, however, the escape velocity is nearly  $38 \text{ km s}^{-1}$  (see the lower curve), i.e.  $v_e > v_s$  (29). Thus only a

tiny fraction of the virialized gas is susceptible to baryonic stripping.

As for the thermal contribution, while the gas on the outskirts of the perturbation is heated above  $T_{\text{vir}}$ , causing the initial rise in the upper curve, the short cooling times in the dense inner regions of the halo prevent  $T > T_{\text{vir}}$  heating at later times. A heating plateau is soon achieved, after which additional baryonic heating becomes negligible. Thus at the end of the simulation ( $t = 58.2$  M yr), only 0.9% of the gas is affected by mechanical evaporation and only 0.7% is supplied with enough momentum to be stripped; hence, the impact of the cosmic blast is trivial.

Figure 6 shows the analogous plots for the pre-virialized halo at the turn-around phase. In this case we find that galaxy formation is strongly affected, as a result of the stronger shock (the Mach number is larger than in the previous case) and the more diffuse structure of the over-dense region, which make the system more vulnerable to the impinging blast. This is particularly evident in the case of baryonic stripping, which increases remarkably (69.9% at the end of the simulation,  $t = 133$  M yr) in comparison with

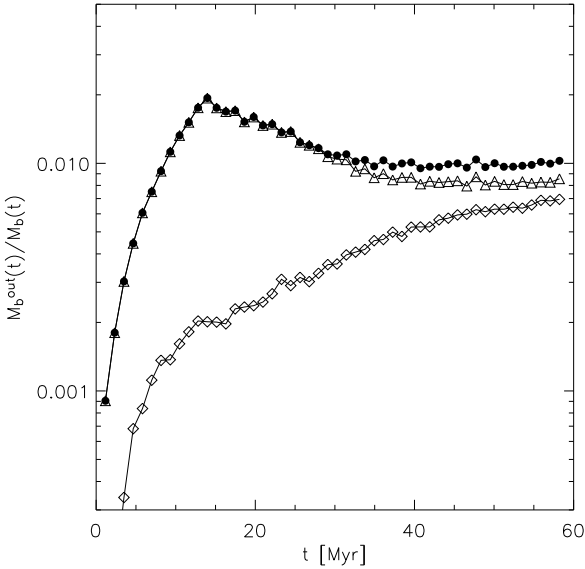


Figure 5. Mass loss in the virialized case. Triangles represent the fraction of mass with  $T > T_{\text{vir}}$ , while the diamonds points give the fraction of mass with  $v > v_e$ . Line with filled circles gives the total fraction of the baryonic mass removed from the virial radius of the halo by both mechanisms.

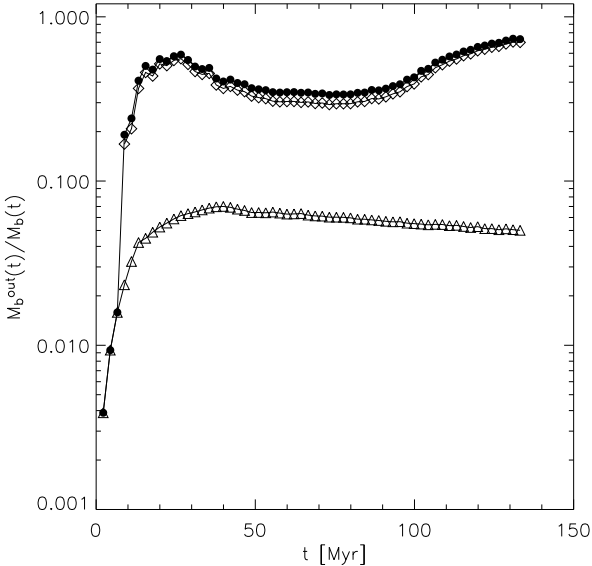


Figure 6. Mass loss in the halo at turn-around. Lines and points are as in Figure 5. Note the difference in scale on the y-axis.

the virialized case. On the other hand the behaviour of the thermal contribution (curve with triangles) is only weakly enhanced with respect to the previous case, attaining a value of  $\sim 5.0\%$  at the final output time.

## 5 SUMMARY AND DISCUSSION

In this paper we have studied the interaction of a cosmic shock wave, generated by multiple supernovae occurring in a primordial galaxy, with a neighbouring halo either already

virialized or at the turn-around stage. The main aim of the investigation is to assess if an intergalactic shock may be able to prevent the collapse of a fraction of dwarf galaxies at high redshifts, thus alleviating the so-called "cooling catastrophe" (for a review of feedback effects see Ferrara & Salvaterra (2004)). We have followed in detail the evolution of the target halo during and after the impact with the supersonic front by means of numerical simulations.

The main results of this study can be summarized as follows. Suppression of dwarf galaxy formation can occur in the collapse stage at or before turn-around. In this case we find that about 70% of the gas can be stripped from the parent halo and ejected into the intergalactic medium. Most of the gas is unbound by the impinging momentum from the shock wave, which is sufficient to accelerate it to velocities larger than the local escape speed. The effects of thermal evaporation of the gas (i.e. due to gas heating by the shock) are found to be negligible in comparison to stripping, in agreement with the conclusions of Scannapieco, Ferrara & Broadhurst (2000).

The effect of the shock wave is much weaker if the halo is already in a virialized state because of the more compact configuration and consequent higher gas density, which enhances radiative losses. The shock removes  $\sim 1\%$  of the gas, and the forming galaxy is hardly affected by the interaction.

As the time spent around turn-around is much longer than the interval from virialization to star formation due to strong radiative losses, we expect the pre-virialized case to be more representative of the majority of outflow-galaxy interactions. Thus SN-driven pregalactic outflows may be an efficient mechanism for inhibiting the formation of neighbouring galaxies at high redshift.

Our numerical experiments have explored two typical situations among the possible shock-target galaxy interactions. However, they are by no means exhaustive. For example we have used mean values in order to choose the target galaxy (mass, formation redshift, density profile) and shock properties (energy, velocity at the interaction). Therefore a full exploration of the likely range for these parameters should be considered, at least for the more interesting case of pre-virialized halos, before a final conclusion on the relevance of these event can be drawn. Additional complications may arise from occurrences of multiple shocks impinging on the same halo, coming from different source galaxies. However, given the relatively short duration of the interaction with the shock (100-200 Myr) the probability that more than one shock at a time is acting on the target galaxy seems unlikely, as this would require remarkable synchronization of the starbursts in different galaxies.

The implications of the suppression effects might be particularly evident in the shape and evolution of the luminosity function. In particular, we expect a selective decrease in the number of low-luminosity objects, due to their inability to collapse and form stars. Our results might also have implications for the number of satellites found around large galaxies, one of the major problems in current hierarchical models of galaxy formation. The baryonic component of these satellites could be destroyed early on by interactions with shocks produced by the first cosmic episodes of star formation. Finally, stripping might drastically change the baryonic-to-dark matter ratios as a function of galactic mass. Although it is likely that SN explosions inside a given

galaxy will affect this observable, our study shows that impinging intergalactic shocks can play an equally important role. We plan to investigate these aspects in forthcoming work.

#### ACKNOWLEDGMENTS

We are grateful to Chris McKee for helpful comments during the preparation of this manuscript. We would also like to thank an anonymous referee for useful discussion. ES was supported by an NSF Math and Physical Sciences Distinguished International Postdoctoral Research (NSF MPS-DRF) fellowship during part of this investigation; his research was also supported by the National Science Foundation under grant PHY 99-07949. We acknowledge partial support from the Research and Training Network "The Physics of the Intergalactic Medium" established by the European Community under the contract HPRN-CT 2000-00126 RG 29185.

#### REFERENCES

- Barkana, R. 2002, *New A*, 7, 85
- Benson, A. J., Lacey, C. G., Frenk, C. S., Cole, S., & Baugh, C. M. 2001, *Bulletin of the American Astronomical Society*, 33, 871
- Benson, A. J., Lacey, C. G., Baugh, C. M., Cole, S., & Frenk, C. S. 2002a, *MNRAS*, 333, 156
- Benson, A. J., Frenk, C. S., Lacey, C. G., Baugh, C. M., & Cole, S. 2002b, *MNRAS*, 333, 177
- Benson, A. J., Frenk, C. S., Baugh, C. M., Cole, S., & Lacey, C. G. 2003, *MNRAS*, 343, 679
- Benson, A. J. & Madau, P. 2003, *MNRAS*, 344, 835
- Bertschinger, E. 1985, *ApJS*, 58, 39
- Bond, J. R., Cole, S., Efsthathiou, G., & Kaiser, N. 1991, *ApJ*, 379, 440
- Bullock, J. S., Kolatt, T. S., Sigad, Y., Somerville, R. S., Kravtsov, A. V., Klypin, A. A., Primack, J. R., & Dekel, A. 2001, *MNRAS*, 321, 559
- Bychkov, K. V. & Pikelner, S. B. 1975, *Soviet Astronomical Letters*, 1, 14
- Cen, R. & Bryan, G. L. 2001, *ApJ*, 546, L81
- Cen, R. & Ostriker, J. P. 1999, *ApJ*, 519, L109
- Ciardi, B., Ferrara, A., Governato, F., & Jenkins, A. 2000, *MNRAS*, 314, 611
- Ciardi, B., Ferrara, A., & White, S. D. M. 2003, *MNRAS*, 344, L7
- Dekel, A. & Silk, J. 1986, *ApJ*, 303, 39
- Edge, A. C. & Stewart, G. C. 1991, *MNRAS*, 252, 414
- Eisenstein, D. & Hu, W. 1999, *ApJ*, 511, 5
- Efstathiou, G. 1992, *MNRAS*, 256, 43P
- Ferrara, A. & Salvaterra, R. 2004, *astro-ph/0406554*
- Gibson, B. K. 1997, *MNRAS*, 290, 471
- Gnedin, N. Y. 2000, *ApJ*, 542, 535
- Keres, D., Katz, N., Weinberg, D. H., & Dave, R. 2004, *MNRAS*, submitted, *astro-ph/0407095*
- Haiman, Z., Rees, M., & Loeb, A. 1997, *ApJ*, 476, 458 (erratum 484, 985)
- Heger, A. & Woosley, S. E. 2002, *ApJ*, 567, 532
- Jones, C. & Forman, W. 1984, *ApJ*, 276, 38
- Klein, R. I., McKee, C. F., & Coella, P. 1994, *ApJ*, 420, 213
- Kogut, A. et al. 2003, *ApJS*, 148, 161
- Lacey, C. & Cole, S. 1994, *MNRAS*, 271, 676
- Larson, R. B. 1974, *MNRAS*, 169, 229
- Mac Low, M. & Ferrara, A. 1999, *ApJ*, 513, 142
- Madau, P., Ferrara, A., & Rees, M. J. 2001, *ApJ*, 555, 92
- Madau, P. & Rees, M. J. 2001, *ApJ*, 551, L27
- Makino, N., Sasaki, S., & Suto, Y. 1998, *ApJ*, 497, 555
- Mo, H. J. & White, S. D. M. 1996, *MNRAS*, 282, 348
- Mo, H. J. & White, S. D. M. 2002, *MNRAS*, 336, 112
- Mori, M., Ferrara, A., & Madau, P. 2002, *ApJ*, 571, 40
- Navarro, J. F., Frenk, C. S., & White, S. D. M. 1997, *ApJ*, 490, 493
- Navarro, J. F. & Steinmetz, M. 1997, *ApJ*, 478, 13
- Pettini, M. & Pagel, B. E. J. 2004, *MNRAS*, 348, L59
- Press, W. H. & Schechter, P. 1974, *ApJ*, 187, 425
- Rauch, M. 1998, *ARA & A*, 36, 267
- Scannapieco, E., Ferrara, A., & Broadhurst, T. 2000, *ApJ*, 536, L11
- Scannapieco, E., & Broadhurst, T. 2001, *ApJ*, 549, 28
- Scannapieco, E., Ferrara, A., & Madau, P. 2002, *ApJ*, 574, 590
- Songaila, A. 2001, *ApJ*, 561, L153
- Springel, V. & Hernquist, L. 2003, *MNRAS*, 339, 289
- Tegmark, M., Silk, J., & Evrard, A. 1993, *ApJ*, 417, 54
- Thacker, R. J., Scannapieco, E., & Davis, M. 2002, *ApJ*, 581, 836
- Theuns, T., Mo, H. J., & Schaye, J. 2001, *MNRAS*, 321, 450
- Thoul, A. A. & Weinberg, D. H. 1996, *ApJ*, 465, 608
- Voit, G. M. 1996, *ApJ*, 465, 548
- White, S. D. M. & Rees, M. J. 1978, *MNRAS*, 183, 341